PORE SCALE NUMERICAL MODELLING OF ELASTIC WAVE DISPERSION AND ATTENUATION IN PERIODIC SYSTEMS OF ALTERNATING SOLID AND VISCOUS FLUID LAYERS

R. Ciz, E.H. Saenger, and B. Gurevich

email: *saenger@geophysik.fu-berlin.de*
keywords: *finite-difference modeling, viscous fluids, Biot theory*

ABSTRACT

Numerical pore-scale simulation of elastic wave propagation is an emerging tool in the analysis of static and dynamic elastic properties of porous materials. Rotated staggered-grid (RSG) finite difference method has proved to be particularly effective in modelling porous media saturated with ideal fluids. Recently this method has been extended to viscoelastic (Maxwell) media, which allows, in particular, simulation of wave propagation in porous solids saturated with Newtonian fluids. To evaluate the capability of the viscoelastic RSG algorithm in modelling wave dispersion and attenuation we perform numerical simulations for an idealized porous medium, namely a periodic system of alternating solid and viscous fluid layers. Simulations are performed for a single frequency of 50 kHz (for shear waves) and 500 kHz (for compressional waves) and a large range of fluid viscosities. The simulation results show excellent agreement with the theoretical predictions. Specifically the simulations agree with the prediction of Biot's theory of poroelasticity at lower viscosities and with the viscoelastic dissipation at higher viscosities. The finite-difference discretization is required to be sufficiently fine for the appropriate sampling of the viscous boundary layer to achieve accurate simulations at the low values of viscosity.

INTRODUCTION

Despite five decades of research into acoustics of porous media, many questions concerning the nature of acoustic attenuation and dispersion in such media remain unresolved. Some of these questions can be addressed by numerical simulations performed on the micro-scale, that is, on the scale of individual pores and grains. This approach, which can be called digital (or computational) rock physics, is increasingly used to model the effect of pores, fractures and fluid on the effective acoustic properties (Roberts and Garboczi, 2000; Arns et al., 2002, Grechka, 2003; Saenger et al., 2004) as well as geometrical, hydraulic and electrical properties of rocks (Schwartz et al., 1994; Spanne et al., 1994; Auzerais et al., 1996; Arns et al., 2001; Keehm et. al., 2004). Until recently, most of the computational methods for effective *acoustic* properties focused on ideally elastic materials saturated with ideal fluids; however understanding of acoustic dissipation requires taking into account the viscosity of the pore fluids.

Recently Saenger et al. (2005) developed viscoelastic rotated staggered grid (VRSG) algorithm that can perform pore-scale simulation of wave propagation in porous materials saturated with Newtonian fluids. The algorithm of Saenger et al. (2005) is essentially an extension to viscous pore fluids of the rotated staggered grid (RSG) finite-difference (FD) method developed by Saenger et al. (2000). The fluid viscosity is included by modelling the pore fluid as generalised Maxwell body (GMB), which in a wide range of viscosities and frequencies is equivalent to a Newtonian fluid.

In order to use VRSG algorithm for the study of wave propagation in porous media, it is necessary to investigate whether this algorithms can accurately simulate known effects in wave propagation in such

media. It is known that attenuation and dispersion of elastic waves in poroelastic media mainly occurs due to the flow of the pore fluid induced by the propagating waves. Such wave-induced fluid flow can occur due to pressure gradients between peaks and troughs in the wave (Biot's global flow (Biot, 1956a,b)), between more compliant and stiff pores (local or squirt flow (Mavko and Jizba, 1991, Dvorkin et al., 1995)) and between regions of lower and higher compliance (mesoscopic flow (Pride and Berryman, 2003)). The global flow attenuation and dispersion can occur in homogeneous single-porosity media described by the classical Biot's equations of poroelaticity (Biot, 1956a,b), and has a peak at the so-called Biot's characteristic frequency

$$\omega_B = \frac{\eta}{\rho_f \kappa},\tag{1}$$

where η and ρ_f are the viscosity and density of the pore fluid, and κ the permeability of the medium. The local flow attenuation is less well understood. While there is no universally accepted model of this phenomenon, it is generally believed that its characteristic frequency is given by

$$\omega_R = \frac{B}{\eta} \left(\frac{b}{a}\right)^n,\tag{2}$$

where B is characteristic rock stiffness, a is characteristic size of the (stiff) pores, $b << a$ is characteristic thickness of compliant pores (cracks) and n is a dimensionless constant usually taken to be equal to 3 (Mavko and Nur, 1975). The characteristic frequency of the mesoscopic attenuation is given by equation (1) with $n = 2$ (Pride et al., 2003). The principle difference between equations (1) and (2) is in the role of fluid viscosity: Increase of fluid viscosity causes an increase of Biot's characteristic frequency but a decrease of the characteristic frequency for local and mesoscopic flow. One can also note that for single porosity medium (that is, a medium where the size of all pores is of the same order of magnitude) $b/a = O(1)$ so that

$$\omega_R = \frac{B}{\eta}.\tag{3}$$

Therefore, for the single-porosity medium frequency ω_R is the same as that for attenuation due to the classical viscoelastic effect, also known as viscous shear relaxation, that is, stiffening of the material due to fluid viscosity at high frequencies. In other words, in single porosity medium local flow attenuation reduces to classical viscoelastic atternuation.

In order to be applicable for a detailed simulations of porous media, VRSG algorithm needs to be able to simulate phenomena with characteristic frequencies given by equations (1) and (2) or (3). To do this, one needs to simulate the dynamic behaviour of a porous medium with VRSG algorithm and compare the results with known expressions for attenuation and dispersion in such media. While explicit expressions are known for global-flow (Biot's) attenuation (Biot, 1956a,b), they are not known for local flow mechanism, which is the least understood.

This problem can be at least partially resolved by considering an idealised porous medium, such as a periodic system of alternating solid and viscous fluid layers. Such a system, although very idealised, is known to possess many features of saturated porous media. In particular, shear and compressional waves propagating in the plane of the layers of such system and polarised in the same plane have exhibit both Biot's and viscoelastic attenuation with characteristic frequencies given by equations (1) and (3), respectively. At the same time, such a layered system represents the only case of a porous medium for which exact expressions for attenuation and dispersion are known. For these reasons the periodic system of alternating solid and viscous fluid layers is ideally suited for testing of the VRSG algorithm.

Recently Saenger et al. (2005) simulated shear wave propagation in a system of solid and fluid layers and showed excellent agreement with the theoretical solution for Biot's global-flow velocity dispersion. The objective of this paper is to expand on the results of (Saenger et al., 2005) in three ways: (1) by performing numerical simulations of compressional as well as shear wave propagation, (2) computing attenuation as well as dispersion of these waves, and (3) comparing the numerical and theoretical results for both global and local-flow mechanisms.

First, we review the exact dispersion equations for such layered systems and give the basic description of VRSG algorithm. Numerical setup and simulation results are presented in the last section followed by conclusions.

THEORETICAL BACKGROUND

Consider a system of periodically alternating solid and fluid layers of period d (Figure 1). The elastic solid has density ρ_s, bulk modulus K_s and shear modulus μ_s. The viscous fluid has density ρ_f, bulk modulus (inverse compressibility) K_f, and dynamic viscosity η. The solid and fluid layer thicknesses are h_s and h_f, respectively, so that $h_s + h_f = d$.

We analyze the propagation of shear and compressional waves in the x direction parallel to the layering, with the displacement in the direction y (for the shear or SH wave) and to x (for the compressional wave), both parallel to the bedding. For a given frequency ω the solutions can be sought in the form of plane waves

$$u_y = u_{y0} \exp i\omega(x/b - t) \tag{4}$$

for the SH-wave and

$$u_x = u_{x0} \exp i\omega(x/c - t) \tag{5}$$
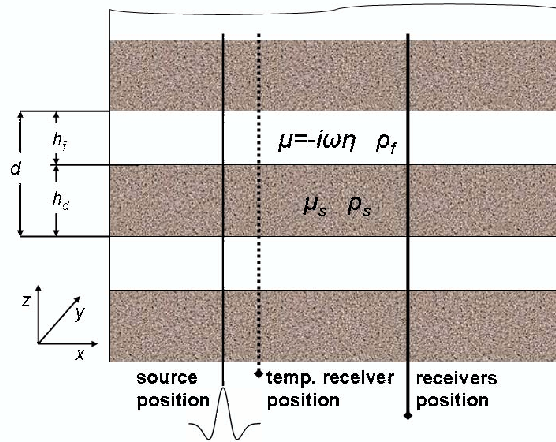
for the P-wave.

Figure 1: Medium of alternating solid and viscous fluid layers.

Shear waves

Propagation of the SH wave in a periodic system of solid and viscous fluid layers is governed by an exact dispersion equation (Rytov, 1956, Brekhovskikh, 1981, Gurevich, 2002a):

$$p \left[\tan^2 \frac{\beta_s h_s}{2} + \tan^2 \frac{\beta_f h_f}{2} \right] + (1 + p^2) \tan \frac{\beta_s h_s}{2} \tan \frac{\beta_f h_f}{2} = 0. \tag{6}$$

Here $\beta_s^2 = \omega^2 \left(1/b_s^2 - 1/b^2 \right)$, $\beta_f^2 = \omega^2 \left(1/b_f^2 - 1/b^2 \right)$, where $b_s = (\mu_s/\rho_s)^{1/2}$, and $b_f = (\mu_f/\rho_f)^{1/2}$ are shear velocities in the materials s and f, respectively, $p = \mu_f \beta_f / \mu_s \beta_s$ and $\mu_f = -i\omega\eta$.

Our aim is to solve the dispersion equation (6) on a macroscale, that is for long waves, to obtain the phase velocities b and c as a function of ω for long waves such that $|\omega d/b| << 1$. In this limiting case equation (6) reduces to (Gurevich, 2002b):

$$\frac{1}{b^2} = \frac{1}{\mu} \left[\rho - \frac{\rho_f^2 \phi^2}{q(\omega)} \right] \left[1 + i\omega/\omega_V \frac{\phi}{1 - \phi} \right], \tag{7}$$

where $\phi = h_f/d$ is the volume fraction of the fluid layers (porosity), $\mu = \mu_s(1-\phi)$ is the static shear modulus of the system, $\rho = (1-\phi)\rho_s + \phi\rho_f$ is the average density, and

$$q(\omega) = \phi\rho_f \left[1 - (i\omega/\omega_B)^{-1/2} \tan (i\omega/\omega_B)^{1/2} \right]^{-1}, \tag{8}$$

is generalized virtual mass coefficient of the layered system. ω_B has the role of characteristic frequency and is given by an equation similar to equation (1):

$$\omega_B = \eta\phi/3\kappa\rho_f = 4\eta/\rho_f h_f^2 \tag{9}$$

with permeability of porous slabs given by (Bedford, 1986)

$$\kappa = \frac{\phi h_f^2}{12}. \tag{10}$$

In turn, ω_V is viscoelastic characteristic frequency, equation (3). According to equation (7), the behaviour of SH-wave velocity dispersion and attenuation in the layered system depends on the ratio ω_B/ω_V. When $\omega_B << \omega_V$, equation (7) reduces to

$$\frac{1}{b^2} = \frac{1}{\mu} \left[\rho - \frac{\rho_f^2\phi^2}{q(\omega)} \right]. \tag{11}$$

The dispersion equation (11) is identical to the dispersion equation for S-waves in a porous medium described by Biot's theory of poroelasticity with permeability (10) and virtual mass coefficient (8), thus confirming the system of solid and fluid layers as a particular (limiting) case of a poroelastic medium. In the opposite case $\omega_B << \omega_V$, we have

$$\frac{1}{b^2} = \frac{1}{\mu} \left[1 + i\omega/\omega_V \frac{\phi}{1-\phi} \right]. \tag{12}$$

This equation describes the standard viscoelastic dispersion (Gurevich, 1999, 2002a).

The theoretical solutions presented above give the complex shear-wave velocity (or slowness) as a function of frequency. Real part of the complex velocity yields the phase velocity of the wave, while the ratio of imaginary to real part of the squared slowness yields the dimensionless attenuation (inverse quality factor)

$$Q_{Sh}^{-1} = \frac{\operatorname{Im} b^{-2}}{\operatorname{Re} b^{-2}}. \tag{13}$$

Compressional waves

Propagation of the P wave in a periodic system of solid layers denoted by s and f is governed by an exact dispersion equation (Rytov, 1956, Brekhovskikh, 1981, Gurevich, 2002a):

$$\begin{aligned}
& 4(\mu_s - \mu_f)^2 K_1 K_2 + \omega^2 \rho_s \left[c^2\rho_s - 4(\mu_s - \mu_f) \right] K_2 \tan \frac{\beta_s h_s}{2} \\
& + \omega^2 \rho_f \left[c^2\rho_f + 4(\mu_s - \mu_f) \right] K_1 \tan \frac{\beta_f h_f}{2} \\
& - \omega^2 \rho_f \rho_s c^2 \left[L_1 \tan \frac{\beta_f h_f}{2} + L_2 \tan \frac{\beta_s h_s}{2} \right] = 0,
\end{aligned} \tag{14}$$

where $\alpha_s^2 = \omega^2 (1/c_s - 1/c)$, $\alpha_f^2 = \omega^2 (1/c_f - 1/c)$ and $c_s = [(K_s + 4\mu_s/3)/\rho_s]^{1/2}$, $c_f = [(K_f + 4\mu_f/3)/\rho_f]^{1/2}$ are compressional velocities in the materials s and f, respectively, $Im\mu_f = Im\lambda_f = -\omega\eta$, $K_f = \lambda_f + 2\mu_f/3$ and

$$\begin{aligned}
K_1 &= \frac{\omega^2}{c^2} \tan \frac{\beta_s h_s}{2} + \alpha_s\beta_s \tan \frac{\alpha_s h_s}{2}, \\
K_2 &= \frac{\omega^2}{c^2} \tan \frac{\beta_f h_f}{2} + \alpha_f\beta_f \tan \frac{\alpha_f h_f}{2}, \\
L_1 &= \frac{\omega^2}{c^2} \tan \frac{\beta_s h_s}{2} - \alpha_f\beta_s \tan \frac{\alpha_f h_f}{2}, \\
L_2 &= \frac{\omega^2}{c^2} \tan \frac{\beta_f h_f}{2} - \alpha_s\beta_f \tan \frac{\alpha_s h_s}{2}.
\end{aligned} \tag{15}$$

Similarly to the shear wave case, equation (6) needs to be analysed on the macroscale, that is in the limit $|\omega d/c| << 1$. However such a theoretical analysis appears to be too involved, and the analytical

solution is only known in the low-frequency limit (Gurevich, 2002a). However it has been shown numerically (Bedford, 1986), that for sufficiently small values of $|\omega d/c|$ attenuation and dispersion predicted by equation (14) are the same as given by Biot's dispersion equation for fast compressional waves in a porous medium with steady state permeability (10) and virtual mass coefficient given by (8). Note that both equation (14) and Biot's theory predict another type of compressional wave, so-called Biot's slow wave. However analysis of this highly dispersive wave is beyond the scope of this paper.

The theoretical expressions summarised in this section will be used for comparison with numerical simulations.

ALGORITHM

To model wave propagation in a solid-fluid mixture, we apply displacement-stress rotated staggered finite-difference grid (Saenger et al., 2000) to solve the elastodynamic wave equation. With a viscoelastic extension (described in detail in Saenger et al., 2005) we are able to model wave propagation in different kinds of porous media.

The theoretical model of viscoelasticity is based on an approach described by Emmerich and Korn (1987). Incorporation of viscosity based on the generalized Maxwell body (GMB) means that Hooke's law is modified:

$$\sigma_{ij} = c_{ijkl}\epsilon_{kl} - \sum_{m=1}^{n} \xi_m^{ij}. \tag{16}$$

In this equation, σ_{ij}, c_{ijkl}, ε_{kl} denote the stresses, the elastic tensor and the strains, respectively. The number of relaxation mechanisms is equal to m. The anelastic functions ξ_m^{ij} are determined by:

$$\dot{\xi}_m^{ij} + \omega_m \xi_m^{ij} = \omega_m \tilde{Y}_m^{ijkl} \varepsilon_{kl}, \tag{17}$$

with $\tilde{Y}_m^{ijkl}$ as the tensors of anelastic coefficients and ω_m as angular relaxation frequencies. The GMB frequency-dependent viscoelastic modulus $C_{ijkl}(\omega)$ can be derived by inserting the Fourier transform of equation (17) into equation (16):

$$C_{ijkl}(\omega) = c_{ijkl} - \sum_{m=1}^{n} \tilde{Y}_m^{ijkl} \frac{\omega_m}{i\omega + \omega_m}. \tag{18}$$

A second order discretization of equation (6) is implemented in the rotated staggered grid algorithm. As a result the anelastic functions ξ_m^{ij} and coefficients $\tilde{Y}_m^{ijkl}$ are located in the center of an elementary FD-cell at the same position as the stress tensor (see Fig 1(d) of Saenger et. al 2000). The exact position of a boundary between two different materials is exactly the bound of the appendant elementary cells.

A compressible viscous fluid (i.e., Newtonian fluid) can be charcterized by the following frequency-dependent elastic moduli:

$$C_{44}(\omega) = \mu(\omega) = i\omega\eta_\mu, \tag{19}$$

$$C_{12}(\omega) = \lambda(\omega) = \lambda(0) + i\omega\eta_\lambda, \tag{20}$$

with $\lambda(\omega)$ and $\mu(\omega)$ as angular-frequency dependent Lamé parameters. For all examples in this paper we assume that the dynamic fluid viscosity η is equal to η_μ and η_λ. However, the key question is how to approximate the viscous behaviour given by equation (19) and (20) with a GMB. The following strategy is based on a Taylor-expansion of equation (18) for $\omega = 0$:

- We use one relaxation mechanism (n=1).
- $\tilde{Y}_1^{44} = c_{44}$. Only in this case it is possible that $C_{44}(0) = 0$.
- In the low frequency range of the GMB for one relaxation mechanism one can determine the wanted fluid-viscosity by using the following relations:

$$\eta_\mu = \frac{1}{i} \left.\frac{\partial C_{44}(\omega, \tilde{Y}_1^{44} = c_{44})}{\partial \omega}\right|_{\omega=0} = \frac{c_{44}}{\omega_1}, \tag{21}$$

$$\eta_\lambda = \frac{1}{i} \left.\frac{\partial C_{12}(\omega)}{\partial \omega}\right|_{\omega=0} = \frac{\tilde{Y}_1^{12}}{\omega_1}. \tag{22}$$

•For $\eta_\mu = \eta_\lambda$ one can show that $\tilde{Y}_1^{12} = c_{44}$. Further, with equation (18), (20) and the known relation $c_{11} = c_{12} + 2c_{44}$ one can derive (for $\omega = 0$):

$$c_{11} = \lambda(0) + 3c_{44}. \tag{23}$$

•For FD approaches it is necessary to take into account the stability criterion. For the rotated staggered grid with FD operators of second order in time and space the following relation is valid (Saenger et al. 2000):

$$\sqrt{\frac{c_{11}}{\rho_{fluid}}} = v_p \leq \gamma, \quad \gamma = \frac{\Delta h}{\Delta t}. \tag{24}$$

•We choose c_{44} with the following restriction [given by the 'stability criterion'-relation (24) and equation (23)]:

$$c_{44} \leq \frac{\gamma^2 \rho_{fluid} - \lambda(0)}{3}. \tag{25}$$

•Together with the choice of the angular relaxation frequency ω_1 one can determine the wanted dynamic viscosity η [compare with equation (21)].

•We choose a source signal in the low frequency range of the applied GMB ($\omega_{source} << \omega_1$).

NUMERICAL SIMULATIONS AND RESULTS

Numerical setup

To obtain effective velocities and attenuation coefficients in layered media we choose the following numerical setup. The full synthetic model contains two horizontal thin layers of viscous fluid and elastic solid of equal size (30x3000 grid points with an interval of Δx=0.0001 m for SH wave and Δx=0.00001 m for P wave). The solid has the P-wave velocity v_p=5100 m/s, S-wave velocity v_s=2944 m/s, density ρ_s=2540 kg/m^3 and viscosity η=0 kg/m.s. For the viscous fluid we always set c_{11}=3.922*10^{11}, c_{44}=1.3*10^{11}, and ρ_f=1000 kg/m^3. The fluid viscosity η is varied with the choice of ω_1 (see equation (21)). To generate a plane SH-wave (Ricker1, f_{dom}=50 kHz, Δt=5e-9 s) or a P-wave (Ricker1, f_{dom}=500 kHz, Δt=5e-10 s), we apply a line source in horizontal or vertical direction and perform the finite-difference simulations with periodic boundary conditions in the same direction. The effective velocity is estimated by measuring the time of the zero-crossing of the plane wave over a distance of 1000 grid points. All computations are carried out with the second order spatial FD operators and with the second order time update.

To obtain attenuation coefficients from simulation data we analyze the amplitude decaying with distance over one wavelength. Based on the constant "Q" model (Knopoff, 1964, Pilant, 1979, Mavko et al., 1998) the attenuation $1/Q$ reads

$$\frac{1}{Q} = -\frac{1}{\pi} \frac{\Delta A}{A} \bigg|_{L_W}. \tag{26}$$

where ΔA is the change in amplitude A over one wavelength "L_W". This methodology is used to derive the attenuation from the numerically simulated waveforms at the distance of one wavelength.

Numerical results

The results of shear wave simulations are summarized in Figures 2a and 2b which show the shear wave velocity and attenuation plotted versus the fluid viscosity. The solid triangles are simulations results, and the solid line is the theoretical solution obtained by numerically solving the exact dispersion equation (6). Also shown are theoretical solution in poroelastic (11) and viscoelastic (12) limits. We observe a very good agreement between the full theoretical solutions and the numerical simulations for almost the full range of viscosities. Up until viscosity of about 3000 kg/ms the numerical solution also agrees with poroelastic (Biot's) solution (11), after which it tends to follow the viscoelastic solution (12). This latter effect is shown only for a relatively narrow range of frequencies, as the viscoelastic solution is only valid as long as the parameter $\omega/\omega_V = \omega\eta/\mu_s$ is small, that is, for viscosities $\eta << \mu_s/\omega$. At higher viscosities when the viscoelastic term begins to dominate, the waves become strongly dispersive and our method of velocity
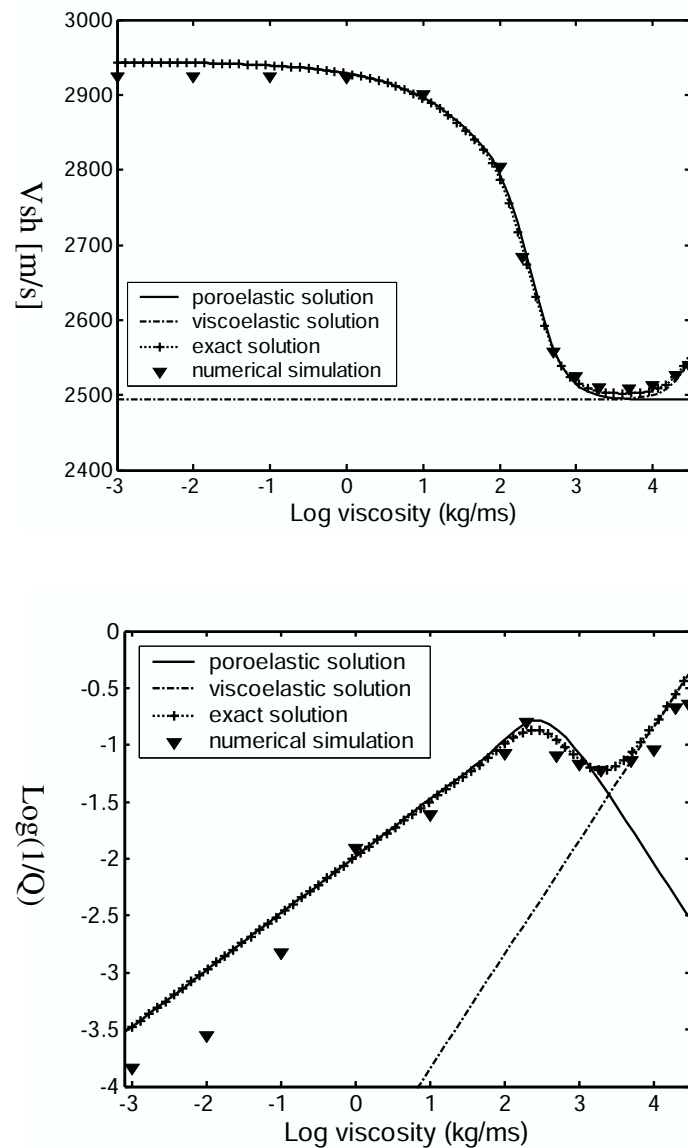
Figure 2: Shear wave velocity (a) and attenuation (b) versus viscosity. The triangles represent values of shear wave velocity obtained from numerical simulations for models with different viscosity values. The cross-dotted line corresponds to exact solution (6), the solid line represents the poroelastic solution (7) and the dash-dotted line denotes the viscoelastic solution (12).

estimation no longer applies. We did not focus on these high viscosities as they are unphysical (in the sense that Newtonian fluid model is no longer valid, see Landau and Lifshitz, 1987). The viscoelastic behaviour is much more clearly visible on attenuation than on the dispersion plot, since the first-order viscoelastic term in (12) is purely imaginary and therefore does not contribute to the phase velocity.

Some small discrepancies are observed for very low and very high viscosities. The discrepancy at low viscosity is likely to be caused by insufficient sampling of the viscous boundary layer near the solid/fluid interface. For instance, at viscosity $\eta = 10 \, \text{kg} / \text{ms}$ and frequency 50 kHz, the thickness of the boundary

layer (viscous skin depth) is already about $(2\eta/\omega\rho_f)^{1/2} = 2.5 \cdot 10^{-4}$m, or about less than 3 grid points of the FD grid. Thus the value $\eta = 10$ kg / m.s is the minimum value of viscosity for which the boundary layer is adequately sampled.
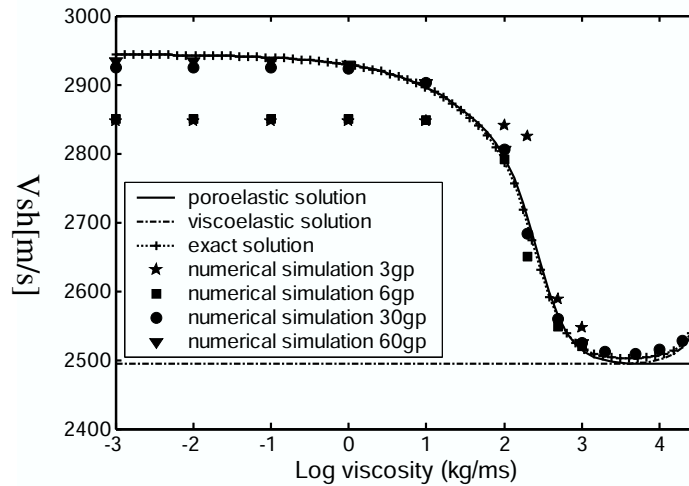

Figure 3: SH-wave velocity versus viscosity. The solid line corresponds to the poroelastic solution (equation 7). The discrete points represent values of SH-wave velocity obtained from numerical simulations for models with varying number of grid points.

To further investigate the relationship between the thickness of the viscous solid/fluid boundary and the number of grid points, the computation of shear velocities was performed for different number of grid points and different size of spatial steps. The results are summarised in Figure 3. These results demonstrate that insufficient spatial sampling causes the observed velocity errors at low viscosities, in situations when the viscous skin depth is small.

The results for P-wave dispersion and attenuation are shown in Figure 4a, b. The numerically simulated values of P-wave velocities (Figure 4a) and inverse quality factor (Figure 4b) are consistent with the exact solution. This agreement is observed in a wide range of viscosities. A small discrepancy appears at viscosities as low as $\eta < 0.1$ kg / m.s. At these very low viscosities the very thin solid/fluid boundary layer is still not properly discretized.

It is useful to note that Biot's theory of poroelasticity neglects the bulk viscosity of the pore fluid. Our numerical simulations include the effects of both bulk and shear viscosities. The theoretical solution for shear waves includes only the effect of shear viscosity. The good agreement between the numerical simulation and the theoretical attenuation and dispersion proves the legitimacy of Biot's assumption as expected. For compressional waves Figures 4a,b show solutions both with $(Im\lambda_f = Im\mu_f = -\omega\eta)$ and without $(Im\lambda_f = 0)$ bulk viscosity. We see that influence of bulk viscosity on the dispersion and attenuation of compressional waves is negligible in the poroelastic regime, and becomes significant only in the viscoelastic regime, again confirming Biot's assumption.

CONCLUSIONS

The main result of this paper is an excellent agreement between the numerical simulations and theoretical predictions of shear and compressional wave velocities and attenuation factors. This agreement is observed in a wide range of fluid visiocities. In the lower viscosity range the solution shows excellent agreement with the poroelastic solution as predicted by Biot's theory of poroelasticity. At higher viscositis the behaviour of velocities and, in particular, attenuation factors is consistent with classical viscoelastic dissipation. This confirms that the viscoelastic rotated staggered grid FD method of Saenger et al. (2005) is capable of modelling both poroelastic (associated with global flow) and viscoelastic effects with high accuracy. The finite-difference discretization required to achieve this accuracy must be sufficiently fine to ensure adequate
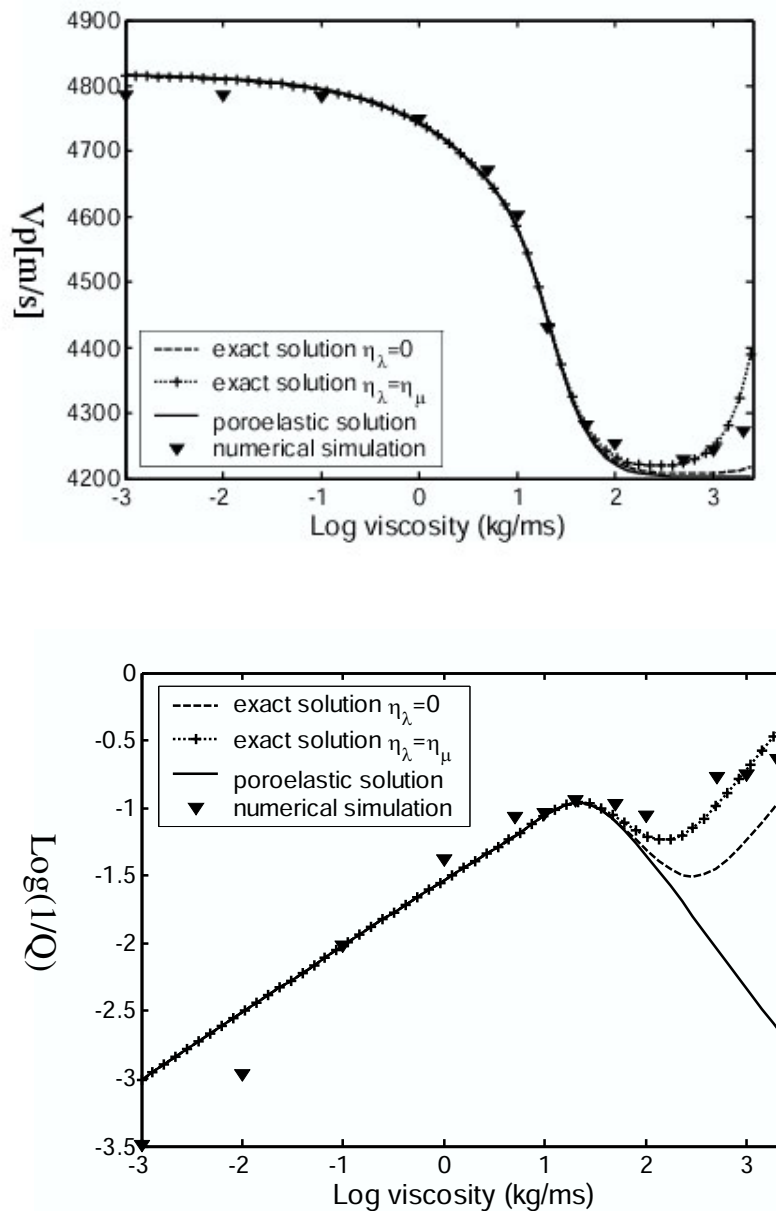
Figure 4: Compressional wave velocity (a) and attenuation (b) versus viscosity. The dashed line corresponds to the exact Rytov's dispersion equation (14) for the case when the bulk viscosity of the fluid layer is neglected. The cross-dotted line represents the exact Rytov's dispersion equation when the solution accounts for the bulk viscosity of the fluid layer. The solid line corresponds to the Biot's dispersion equation for compressional waves. The triangles represent values of compressional wave velocity obtained from numerical simulations for models with varying viscosities for spatial step $\Delta x = 1e - 5$.

sampling of viscous boundary layer near the pore wall. At least two grid points with spatial distance less than the viscous skip depth are required for the accurate computation.

ACKNOWLEDGMENTS

REFERENCES

Arns, C. H., Knackstedt, M. A., Pinczewski,W.V., and Garboczi, E.G. (2001). Accurate estimation of transport properties from microtomographic images, *Geophys. Res. Lett.*, 28, 3361-3364.

Arns, C.H., Knackstedt, M.A., Pincewski, W.V. and Garboczi, E.J. (2002). Computation of linear elastic properties from microtomographic images: Methodology and agreement between theory and experiment, *Geophysics*, 67, 1396-1405.

Auzerais, F. M., Dunsmuir, J., Ferreol, B. B., Martys, N., Olson, J., Ramakrishnan, T. S., Rothman, D. H., and Schwartz, L. M. (1996). Transport in sandstone: A study based on three dimensional microtomography, *Geophys. Res. Lett.*, 23, 705-708.

Bedford, A. (1986). Application of Biot's equations to a medium of alternating fluid and solid layers, *J. Wave-Material Interaction*, 1, 34-53

Biot, M.A. (1956a). Theory of propagation of elastic waves in a fluid-saturated porous solid. I. Low-frequency range, *J. Acoust. Soc. Am.*, 28, 168-178

Biot, M.A. (1956b). Theory of propagation of elastic waves in a fluid-saturated porous solid. II. Higher frequency range, *J. Acoust. Soc. Am.*, 28, 179-191.

Brekhovskikh, L. M. (1981). Waves in layered media *(Academic Press)*.

Dvorkin, J., Mavko, G., and Nur, A. (1995). Squirt flow in fully saturated rocks, *Geophysics*, 60, 97-107.

Emmerich, H. and Korn, M. (1987). Incorporation of attenuation into time-domain computations of seismic wavefields, *Geophysics*, 52, 1252-1264.

Grechka, V., (2003). Effective media: A forward modeling view, *Geophysics*, 68, 2055-2062.

Gurevich, B. (1999). Low-frequency shear wave propagation in periodic systems of alternating solid and viscous fluid layers, *J. Acoust. Soc. Am.*, 106, 57-60.

Gurevich, B. (2002a). Effect of fluid viscosity on elastic wave attenuation in porous rocks, *Geophysics*, 67, 264-270.

Gurevich, B. (2002b). Elastic wave attenuation in porous rocks: Effects of pore fluid viscosity and frequency, *72nd Ann. Internat. Mtg: Soc. of Expl. Geophys.*, 1821-1824.

Keehm, Y., T. Mukerji, and A. Nur (2004). Permeability prediction from thin sections: 3D reconstruction and lattice-boltzmann flow simulation, *Geophys. Res. Lett.*, 31, L04,606.

Knopoff, L. (1964). Q, *Rev. Geophys.*, 2, 625-660.

Landau, L., Lifshitz, E. (1987). Fluid mechanics *(Pergamon press, Inc)*.

Mavko, G., and Jizba, D. (1991). Estimating grain-scale fluid effects on velocity dispersion in rocks, *Geophysics*, 56, 1940-1949.

Mavko, G., Mukerji, T. and Dvorkin, J. (1998). The Rock Physics Handbook *(Cambridge University Press)*.

Pilant, W.L. (1979). Elastic waves in the Earth *(Elsevier Inc)*.

Pride, S. R., Harris, J., Johnson, D. L., Mateeva, A., Nihei, K., Nowack, R. L., Rector, J., III, Spetzler, H., Wu, R., Yamomoto, T., Berryman, J. and Fehler, M. (2003). Permeability dependence of seismic amplitudes, *The Leading Edge*, 22, No. 6, 518-525.

Pride, S.R., and Berryman, J.G. (2003). Linear dynamics of double-porosity double-permeability materials, I. Governing equations and acoustic attenuation, *Physical Review E*, 68 (3), 036603-1 - 036603-10.

Roberts, A. P., and Garboczi, E. J. (2000). Elastic properties of model porous ceramics, *J. Amer. Ceramic Soc.*, 83, 3041-3048.

Rytov, S.M., (1956). Acoustical properties of a thinly laminated medium, *Sov. Phys. Acoust.*, 2, 68-80.

Saenger, E.H., Ciz, R., and Gurevich, B., Pore scale numerical simulations of shear wave dispersion in an idealized porous medium, *Geophys. J. Int.*, submitted.

Saenger, E.H., Gold, N., and Shapiro, S.A. (2000). Modeling the propagation of elastic waves using a modified finite-difference grid, *Wave Motion*, 31, 77-92.

Saenger, E.H., Keehm, Y., and Shapiro, S.A. (2005). Seismic effects of viscous Biot-coupling: Finite difference simulations on micro-scale, *Geophys. Res. Lett.*, L14310.

Saenger, E.H., Krüger, O.S., and Shapiro, S.A. (2004). Numerical considerations of fluid effects on wave propagation: Influence of the tortuosity," *Geophys. Res. Lett.*, L21613.

Schwartz, L. M., Auzerais, F. M., Dunsmuir, J., Martys, N., Bentz, D. P., and Torquato, S. (1994). Transport and diffusion in three-dimensional composite media, *Physica A*, 207, 28-36.

Spanne, P., Thovert, J., Jacquin, J., Lindquist, W. B., Jones, K., and Coker, D. (1994). Synchotron computed microtomography of porous media: Topology and transports, *Phys. Rev. Lett.*, 73, 2001-2004.